Chinese Chemical Letters 33 (2022) 344–348

Contents lists available at ScienceDirect

Chinese Chemical Letters

journal homepage: www.elsevier.com/locate/cclet

Nitrogen and boron co-doped graphene nanoribbons as peroxidase-mimicking nanozymes for enhanced biosensing

Siyu Luo[a], Meng Sha[b], Fei Tian[a], Xialian Li[a], Lijie Fu[a], Yingqiu Gu[a], Lu-Lu Qu[a,*], Guo-Hai Yang[a,*], Chengzhou Zhu[b,*]

[a] School of Chemistry & Materials Science, Jiangsu Normal University, Xuzhou 221116, China
[b] Key Laboratory of Pesticide and Chemical Biology of Ministry of Education, International Joint Research Center for Intelligent Biosensing Technology and Health, College of Chemistry, Central China Normal University, Wuhan 430079, China

ARTICLE INFO

Article history:
Received 3 March 2021
Revised 8 April 2021
Accepted 4 June 2021
Available online 17 June 2021

Keywords:
Graphene nanoribbons
Heteroatom doping
Nanozymes
Biosensing
Interleukin-6

ABSTRACT

The rational design of nanozymes with superior activities is essential for improving bioassay performances. Herein, nitrogen and boron co-doped graphene nanoribbons (NB-GNRs) are prepared by a hydrothermal method using urea as the nitrogen source and boric acid as the boron source, respectively. The introduction of co-doped and edge structures provides high defects and active sites. The resultant NB-GNRs nanozymes show superior peroxidase-like activities to nitrogen-doped and boron-doped counterparts due to the synergistic effects. By taking advantage of their peroxidase-like activities, NB-GNRs are used for the first time to develop enzyme-linked immunosorbent assay for the detection of interleukin-6. The biosensors exhibit a high performance with a linear range from 0.001 ng/mL to 1000 ng/mL and a detection limit of 0.3 pg/mL. Due to their low cost and high stability, the proposed nanomaterials show great promise in biocatalysis, immunoassay development and environmental monitoring.

Nanozymes are biomimetic nanomaterials that exhibit activities similar to natural enzymes, *e.g.*, horseradish peroxidase (HRP) can be substituted by a nanozyme with peroxidase-like activity. Nanozymes have attracted wide attention due to their large-scale preparation capabilities and good stabilities. Since 2007, when Fe_3O_4 nanomaterials were first used to mimic intrinsic peroxidase-like activity [1], researchers have made great progress with nanozymes in the past decade [2]. Metal oxides [1,3–7], noble metals [8–10] and other nanomaterials [11–15] have been extensively studied in this area. It is noted that the catalytic activities of some metal oxide-based nanozymes are not satisfactory with low affinity in general [16,17]. Noble metals generate high peroxidase capabilities, while the cost is high. Moreover, they tend to have oxidase capabilities and can oxidize substrates in the absence of hydrogen peroxide (H_2O_2) [10,18]. Multi-enzyme-like activities seriously impede the availability of nanozymes in practical applications. Therefore, developing advanced nanozymes with high catalytic activity and selectivity, and low cost is greatly needed.

The peroxidase-like activity of carbon-based nanomaterials has also been extensively investigated [19–21]. In addition to ease of mass production, their surfaces containing rich functionalities are ideal for conjugating antibody molecules [22–24]. Therefore, carbon nanomaterials are promising alternative for natural enzymes in the field of biosensing. However, the practical applications of carbon nanozymes are hindered by the drawbacks of low catalytic activity. Further boosting their catalytic activities is one of the most important considerations. Graphene nanoribbons (GNRs) are graphene derivatives characterized by nanometer-wide strips, high electron transport performances and large specific surface areas. GNRs have special edge limiting effects, which make them more flexible and adjustable, thereby increasing their practical value [25–27]. GNRs can be prepared by stripping and reducing multi-walled carbon nanotubes (MWCNTs) in a specific direction. Meantime, GNRs can be modified with abundant oxygen-containing groups to improve the dispersibility in aqueous solutions, which are also beneficial to the coupling of antibody molecules [28]. Moreover, the open-edge-normalized activity of graphene-based materials is higher than that of basal planes [29]. On the other hand, chemical doping effectively regulates the surface structure and electrical properties of carbon-based nanomaterials, holding great promise in synthesizing functional materials. For example, in recent years, several studies have observed that doped carbon, graphene and graphene quantum dots have wide applications in batteries, capacitors, photocatalysis and biosensors [30–35].

* Corresponding authors.
E-mail addresses: luluqu@jsnu.edu.cn (L.-L. Qu), yangguohai@jsnu.edu.cn (G.-H. Yang), czzhu@mail.ccnu.edu.cn (C. Zhu).

https://doi.org/10.1016/j.cclet.2021.06.018
1001-8417/

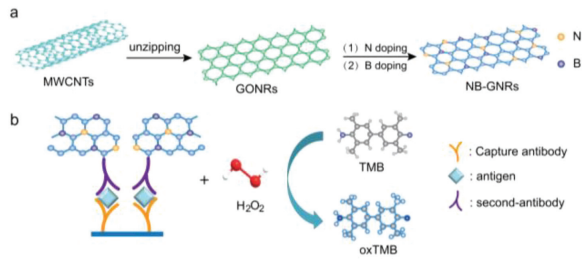

Fig. 1. Schematic diagram of NB-GNRs nanozymes synthesis (a) and schematic illustration for colorimetric detection of IL-6 (b).

Specifically, heteroatoms have also been used to enhance the enzyme-like activity of carbon nanomaterials via their synergistic actions [20,36,37]. Therefore, accurate synthesis of heteroatom-doped GNRs and further exploration of their enzyme-like activity provide great opportunities for their potential applications in biosensing. As far as we known, the research on enzyme-like activities of doped GNRs has not been explored.

Herein, nitrogen and boron co-doped graphene nanoribbons (NB-GNRs) were synthesized using a hydrothermal method, using urea and boric acid as nitrogen and boron sources, respectively. The synergistic effects of co-doped and edge structures of NB-GNRs appeared to boost the intrinsic activity of carbon nanozymes. The resultant NB-GNRs exhibited superior peroxidase-like activity with a strong affinity for H_2O_2 and 3,3′,5,5′-tetramethylbenzidine (TMB), while no oxidase-mimicking activity which would be free from disturbance of O_2 for the assay system. Furthermore, nitrogen and boron doping levels were controlled by boron and nitrogen source levels and the optimized NB-GNRs with the best peroxidase-like activity were achieved when the ratio of graphene oxide nanoribbons (GONRs), urea and boric acid at a 1:10:10 (Fig. 1a). By taking advantage of their superior peroxidase-like activities, NB-GNRs were used to fabricate efficient and sensitive colorimetric quantitative detection assays for interleukin-6 (IL-6) (Fig. 1b), which exemplifies the practical feasibility of NB-GNRs as nanozymes for bioassay systems.

To obtain high-quality NB-GNRs, GONRs were first synthesized by the longitudinal unzipping of MWCNTs [38], and NB-GNRs were synthesized by a two-step hydrothermal method. This strategy reduced the generation of low active components. A dark, homogeneous NB-GNRs solution was generated after a short reaction time which can be stable for up to 8 months without any visible precipitate (Fig. 2a). The corresponding contact angle measurement showed that NB-GNRs instantaneously absorbed water in 2 s without contact angle (Fig. 2a), indicating good hydrophilicity of NB-GNRs [39]. Abundant carboxylic groups and intermolecular electrostatic repulsion in the network play a key role in preventing both inter- and intra- π-π stacking of GNRs, resulting in good dispersibility [40]. As expected, the ζ-potential of NB-GNRs in water was measured at -44.5 ± 2.8 mV, larger than those of GNRs, N-GNRs and B-GNRs (Fig. S1 in Supporting information), suggesting that NB-GNRs had a better dispersibility and stability in aqueous solution, which was consistent with the contact angle data. Heteroatom co-doped GNRs increases the defects of GNRs [18], thus improving the dispersion of GNRs, which is beneficial for the application of NB-GNRs in biosensors.

NB-GNRs morphologies were characterized by scanning electron microscopy (SEM) and transmission electron microscopy (TEM). SEM images show that the diameter of MWCNTs is approximately 20–30 nm (Fig. S2a in Supporting information), and the width of NB-GNRs is approximately 80–100 nm (Fig. 2b). These images reveal that after the longitudinal unzipping of MWCNTs, the tube walls open to produce GONRs (Fig. S2 in Supporting information).

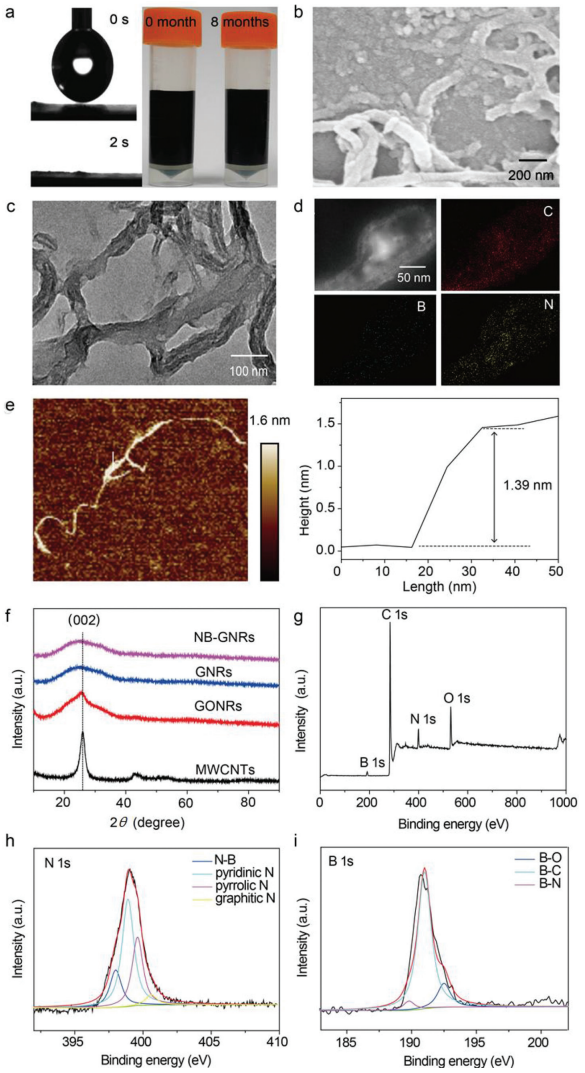

Fig. 2. (a) Contact angle of NB-GNRs (left), and digital photos of the solutions of NB-GNRs (right). SEM (b) and TEM (c) images of NB-GNRs. (d) HADDF-STEM image of NB-GNRs and the corresponding element mapping images. (e) AFM image (left) and cross-section analysis (right) along with the line in AFM image of NB-GNRs. (f) XRD patterns of MWCNTs, GONRs, GNRs and NB-GNRs. (g) XPS spectrum of NB-GNRs, the corresponding high-resolution XPS spectra of N 1s (h) and B 1s (i).

These hollow tubular structures of MWCNTs were observed in TEM images (Fig. S2d in Supporting information), while the lateral wall of NB-GNRs was expanded to form a banded structure, without a hollow core (Fig. 2c). These observations indicated that NB-GNRs were successfully synthesized. Equally, the morphology of GNRs did not change during reduction and doping (Fig. S2 in Supporting information). High-angle annular dark-field scanning transmission electron microscopy (HADDF-STEM) image, and the corresponding elemental mapping images (Fig. 2d) show that N, B and C are uniformly distributed among the GNRs network, indicating these heteroatoms were successfully doped in GNRs. Atomic force microscopy (AFM) image further show that NB-GNRs possess the nanoribbon shape with approximately 1.39 nm thick, confirming a monolayer carbon structure (Fig. 2e).

The structural properties of NB-GNRs were characterized by X-ray powder diffraction (XRD) (Fig. 2f). A graphitization peak (002) was observed at 26.1° in the MWCNTs sample. After the longitudinal decompressing, the graphitized peaks of GONRs became wider and slightly sharper, indicating that MWCNTs had successfully unzipped. After the hydrothermal reaction, the graphitized peaks of

GNRs and NB-GNRs became weak and wide. This was mainly due to the reduction of the graphite layer, and peak strength after heat treatment [41–43].

X-ray photoelectron spectroscopy (XPS) spectra show the existence of C, N and B of BN-GNRs (Figs. 2g–i and Fig. S3 in Supporting information), achieving heteroatom-doping in the GNRs framework and surrounding C atoms (Fig. 2g). The C 1s band was deconvoluted into three bands at 284.7 eV, 286.2 eV, and 288.5 eV, corresponding to C—C, C—N and C—O bonds, respectively (Fig. S3). The broad N 1s band was deconvoluted into four bands at 398.0 eV, 398.9 eV, 399.6 eV and 400.6 eV, assigned to N-B, pyridinic N, pyrrolic N and graphitic N bonding structures, respectively (Fig. 2h) [44,45]. The B-moieties in NB-GNRs products existed as B—N, B—C and B—O bonds, and their corresponding deconvoluted energy bands were 189.8 eV, 191.0 eV and 192.5 eV, respectively (Fig. 2i) [46]. For comparison, N-GNRs, B-GNRs, NB-GNRs (1:5:5) and NB-GNRs (1:15:15) were also prepared. The results further showed C, B, N and O were contained in NB-GNRs, and that N and B contents could be facilely tuned by controlling the ratio of boric acid and urea (Table S1 in Supporting information). Significantly, the content of heteroatoms (N, B and O) of NB-GNR is about 18.7%, higher than those of N-GNRs (13.05%) and B-GNRs (15.52%). The introduction of heteroatoms and aboundant edge structures in NB-GNRs provided more active sites and defects, which would be beneficial for their enhanced catalytic activity. It was also found the oxygen-containing groups in NB-GNRs were maintained during hydrothermal treatment. These groups facilitated not only the conjugation of the antibody, but also their good dispersion in the aqueous solution.

Then, we investigated the peroxidase-like activity of NB-GNRs using TMB as a substrate. In the presence of H_2O_2, NB-GNRs rapidly oxidized TMB and produced distinct color changes with a characteristic absorption peak at 652 nm, while no color changes were observed for TMB/H_2O_2 and TMB/NB-GNRs systems (Fig. 3a). These results showed that NB-GNRs exhibited excellent peroxidase-like activity, and could oxidize TMB in the presence of H_2O_2. Note that NB-GNRs had no oxidase-like activity, and the peroxidase-mimicking performance of NB-GNRs could be free from O_2 interference. Furthermore, the peroxidase-like activities of the different materials including GONRs, GNRs, N-GNRs, B-GNRs and NB-GNRs were also compared (Fig. 3b). As expected, NB-GNRs exhibited the highest peroxidase-like activity. Besides, the resultant NB-GNRs nanozymes also had good stability (Fig. S4 in Supporting information). Electron paramagnetic resonance (EPR) was used to detect radicals produced during the NB-GNRs catalytic process (Fig. 3c). DMPO was used to capture radicals in the reaction. When DMPO was added to H_2O_2 without NB-GNRs as capture radicals in the reaction, no characteristic peak generated. When NB-GNRs were mixed with H_2O_2, four peaks were observed in the EPR spectrum with the intensity ratio of 1:2:2:1, consistent with DMPO-•OH [47–49]. The optimized catalyst concentration (20 μg/mL NB-GNRs), pH (4.0) and temperature (37 °C) for NB-GNRs were obtained (Fig. S5 in Supporting information). Besides, the effect of heteroatom doping ratio was investigated and it was found that the optimized NB-GNRs with the feeding ratio of GONRs, urea and boric acid at a 1:10:10 exhibited the best activity. The enhanced activity of NB-GNRs (1:10:10) was supported by the results from Raman spectroscopy (Fig. S6 in Supporting information). The I_D/I_G value of NB-GNRs (1:10:10) was higher than those of NB-GNRs (1:5:5), NB-GNRs (1:15:15), N-GNRs and B-GNRs, exhibiting a higher degree of disorder and defects, which were beneficial to their enhanced nanozyme catalytic activity [50].

To further explore catalytic effects, reaction steady-state kinetic parameters were determined using NB-GNRs as a catalyst. According to Beer-Lambert's law, the molar absorbance coefficient of the oxidation product derived from TMB was 39,000 L mol^{-1} cm^{-1},

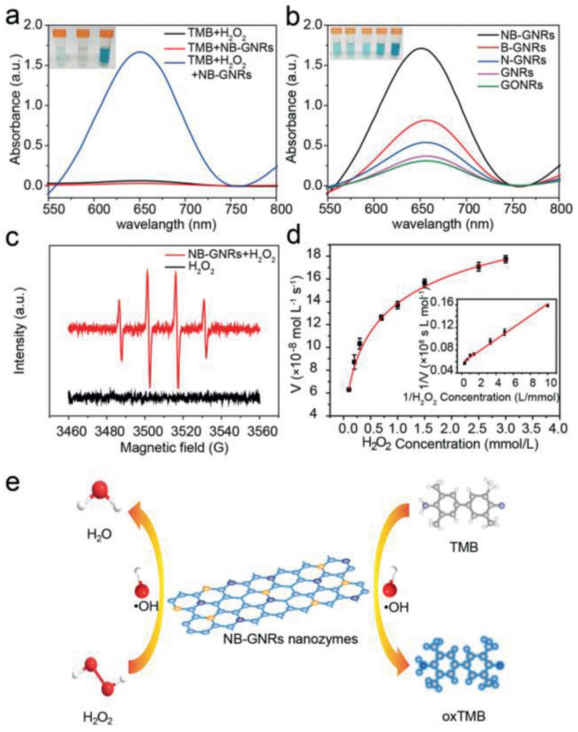

Fig. 3. (a) UV–vis absorption spectra of TMB + H_2O_2, TMB + NB-GNRs and TMB + H_2O_2 + NB-GNRs (from left to right). (b) UV–vis absorption spectra of different nanozymes (from left to right: GONRs, GNRs, N-GNRs, B-GNRs, NB-GNRs). Photographs (top) of the color-generating reaction of TMB in the presence of H_2O_2, and (bottom) their corresponding absorption spectra. (c) EPR spectrum of NB-GNRs + H_2O_2 + DMPO and H_2O_2 + DMPO. (d) Michaelis–Menten kinetics curves for H_2O_2. Inset: Lineweaver–Burk plots (The error bars represent the standard deviations from parallel determination of five duplicate assays). (e) Schematic illustration of the mechanism of enhanced nanozyme activity of NB-GNRs.

and the rate of change of absorbance is converted to the rate of change of concentration to obtain the reaction rate. The reaction catalyzed by NB-GNRs conformed to Michaelis-Menten kinetics. This equation $V_0 = V_{max} \times [S]/(K_m + [S])$, stated that V_0 is the initial velocity, V_{max} is the maximum reaction velocity, K_m is the Michaelis-Menten constant, and [S] is the substrate concentration. V_{max} and K_m were calculated from the slope and intercept of the double reciprocal curve (Fig. 3d). Using these calculations, the K_m of NB-GNRs with H_2O_2 was 0.169 mmol/L, while the value of K_m for NB-GNRs to TMB was 0.193 mmol/L (Fig. S7 in Supporting information). The K_m is inversely related to the affinity of the substrate for the enzyme. NB-GNRs nanozymes had higher V_{max} and smaller K_m than those of N-GNRs and B-GNRs nanozymes (Figs. S8 and S9 in Supporting information). These results indicated that NB-GNRs exhibited a stronger affinity for the substrate and higher peroxidase-like activity. K_m and V_{max} values of NB-GNRs were also superior to those of natural enzymes and some other nanozymes (Table S2 in Supporting information). It is proposed that the synergistic effects of co-doped and edge structures play a key role in tuning defects and enhancing the intrinsic activity of active sites, which improve the electron transfer during catalytic reactions, thereby increasing their nanozyme activity [36,51,52]. These factors contributed to the excellent performance of NB-GNRs nanozymes (Fig. 3e).

The abnormal expression of IL-6 is detected in multiple myeloma and leukemia, and is used as a biomarker for leukemia [53]. IL-6 was detected by conventional sandwich immunoassay [54], in which the antibody-conjugated NB-GNRs were specifically bound to IL-6 molecules in samples. By adding H_2O_2 and TMB, NB-GNRs catalyzed the oxidation of TMB, to produce a blue color.

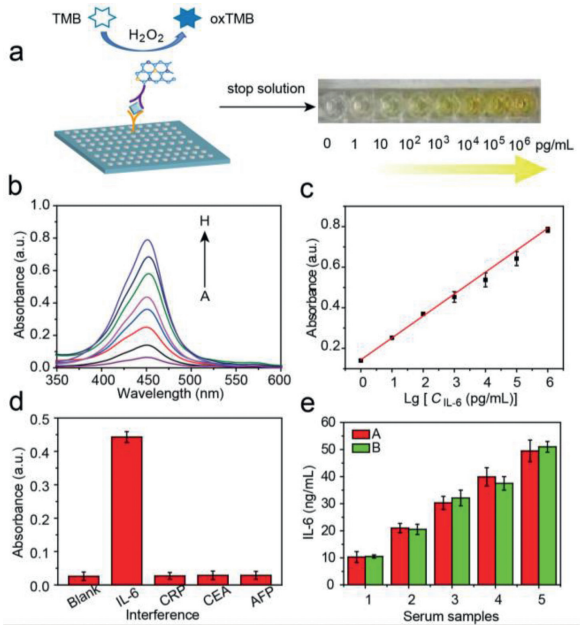

Fig. 4. (a) Schematic illustration of NB-GNRs nanozyme-based IL-6 biosensing. (b) Absorption spectra of the NB-GNRs based immunoassay for IL-6 detection with different concentrations (from A to H: 0, 1, 10, 10^2, 10^3, 10^4, 10^5 and 10^6 pg/mL). (c) The corresponding relationship between peak intensity and IL-6 concentrations. (d) Possible interferences tested with the NB-GNR-based immunoassay. (e) Comparison of serum IL-6 levels determined using NB-GNRs-based immunoassay (A) and HRP-based ELISA method (B).

Therefore, IL-6 could be detected using NB-GNRs as a viable alternative to HRP for immunoassays. IL-6 antibodies were easily coupled to the NB-GNRs surface using abundant carboxyl residues. It was found the antibody-coupled NB-GNRs could effectively retain its original catalytic activity. The blue color, corresponding to oxidized TMB, was rapidly observed in wells containing IL-6. After a 5 min reaction time, the solution turned from blue to yellow upon addition of the stop solution, revealing the high potential of the NB-GNRs-based immunoassay (Fig. 4a). As shown in Fig. 4b, the absorbance intensity at 450 nm increased with the concentration of IL-6 increased. A good linear relationship of 0.001 ng/mL to 1000 ng/mL was observed (Fig. 4c). The linear regression equation was $A = 0.144 + 0.108 \lg C$ (A represents absorbance intensity, and C is the concentration of IL-6 antigen, pg/mL) with a correlation coefficient of 0.9989. The limit of detection (LOD) (S/N = 3) was 0.3 pg/mL, which was better than that of the HRP-based ELISA method. The proposed strategy also showed a wider linear range and a lower detection limit than those of some other methods (Table S3 in Supporting information). It was believed that the favorable active sites with enhanced catalytic endurance provided by the NB-GNRs improve the biosensing performance.

Specificity is an important criterion for any analytical tool. Other proteins such as carcinoembryonic antigen (CEA), C-reactive protein (CRP) and alpha-fetoprotein (AFP) were used as interference molecules to evaluate assay specificity, by comparing the colorimetric responses of 1.0 ng/mL IL-6 solution with the same solution containing an additional interferential substance of 100 ng/mL. The colorimetric response changes for CEA, CRP and AFP were 8.5%, 9.0% and 9.1%, respectively (Fig. 4d). These data indicated that our sensor was highly selective for IL-6, and could be capable of distinguishing IL-6 from the interferences in complex samples. The colorimetric assay also showed good reproducibility at one IL-6 level for five replicate measurements with relative standard deviations (RSD) of 3.8%. When immunosensors were stored at 4 °C for > two months, the signals retained approximately 93.5% of their colorimetric response, indicating the immunosensor had acceptable stability. The feasibility in clinical applications was also investigated by analyzing several real samples for IL-6, and then comparing the data with an HRP-based ELISA assay. As shown in Fig. 4e, the RSD between NB-GNRs-based immunoassay and the HRP-based ELISA method ranged from −6.5% to 7.2%. These data indicated no significant differences between these data, thus our immunoassay may be an alternative tool for protein detection in clinical laboratories.

Based on the excellent peroxidase-mimicking properties of NB-GNRs, glucose was also successfully detected by the NB-GNRs-TMB-GO_x system. As the glucose concentration increased from 2 μmol/L to 240 μmol/L, the absorbance at 652 nm also increased, and the color gradually changed to blue (Figs. S10a and b in Supporting information). Accordingly, we observed a strong linear relationship between the absorbance and glucose concentrations in the range 2–240 μmol/L. The LOD was as low as 0.22 μmol/L (Fig. S10c in Supporting information), which was better than other studies reporting the colorimetric detection of glucose (Table S4 in Supporting information). A series of interference molecules (*i.e.*, fructose, lactose, mannose, ascorbic acid and dopamine) were used to assess the anti-interference ability of the biosensor (Fig. S10d in Supporting information). It was found that the interference molecules and the blank did not show this absorption peak, indicating the sensor was highly selective and sensitive for glucose.

In summary, NB-GNRs were successfully synthesized using a simple hydrothermal reaction. The NB-GNRs acted as the novel carbon-based nanozymes with enhanced peroxidase-like activity without oxidase activity, avoiding the influence of oxygen. Due to the synergistic effects of co-doped and edge structures, the catalytic efficiency of NB-GNRs was considerably improved. NB-GNRs had a good linear range for glucose and IL-6 bioassay with low LOD. Our work demonstrated the feasibility of using NB-GNRs to sensitively and easily identify biomolecules. Therefore, due to their structural characteristics and high peroxidase-like activity, NB-GNRs hold great promise in the biomedical field.

Declaration of competing interest

The authors declare that they have no known competing financial interests or personal relationships that could have appeared to influence the work reported in this paper.

Acknowledgments

This work was supported by the National Natural Science Foundations of China (Nos. 21605062, 21974055); the Top-notch Academic Programs Project of Jiangsu Higher Education Institution (TAPP).

Supplementary materials

Supplementary material associated with this article can be found, in the online version, at doi:10.1016/j.cclet.2021.06.018.

References

[1] L. Gao, J. Zhuang, L. Nie, et al., Nat. Nanotechnol. 2 (2007) 577–583.
[2] J. Wu, X. Wang, Q. Wang, et al., Chem. Soc. Rev. 48 (2019) 1004–1076.
[3] Q. Chen, X. Zhang, S. Li, et al., Chem. Eng. J. 395 (2020) 125130.
[4] R. Andre, F. Natalio, M. Humanes, et al., Adv. Funct. Mater. 21 (2011) 501–509.
[5] N. Singh, M.A. Savanur, S. Srivastava, P. D'Silva, G. Mugesh, Angew. Chem. Int. Ed. 56 (2017) 14267–14271.
[6] X. Liang, L. Han, Adv. Funct. Mater. 30 (2020) 2001933.
[7] J. Li, Y. Cao, S.S. Hinman, et al., Biosens. Bioelectron. 100 (2018) 304–311.
[8] X. Xu, L. Wang, X. Zou, et al., Sens. Actuator. B: Chem. 298 (2019) 126876.
[9] O. Adeniyi, S. Sicwetsha, P. Mashazi, ACS Appl. Mater. Interfaces 12 (2020) 1973–1987.
[10] L. Jiao, L. Zhang, W. Du, et al., Nanoscale 11 (2019) 8798–8802.
[11] W. Zhang, S. Hu, J.J. Yin, et al., J. Am. Chem. Soc. 138 (2016) 5860–5865.

[12] P. Zhang, D. Sun, A. Cho, et al., Nat. Commun. 10 (2019) 940.
[13] B. Tan, H. Zhao, W. Wu, et al., Nanoscale 9 (2017) 18699–18710.
[14] Y. Zhong, X. Tang, J. Li, et al., Chem. Commun. 54 (2018) 13813–13816.
[15] Y. Zhong, J. Li, A. Lambert, Z. Yang, Q. Cheng, J. Mater. Chem. B 7 (2019) 7257–7266.
[16] J. Mu, Y. Wang, M. Zhao, L. Zhang, Chem. Commun. 48 (2012) 2540–2542.
[17] L. Han, H. Zhang, D. Chen, F. Li, Adv. Funct. Mater. 28 (2018) 1800018.
[18] M.I. Kim, Y. Ye, M.A. Woo, J. Lee, H.G. Park, Adv. Healthc. Mater. 3 (2014) 36–41.
[19] W. Shi, Q. Wang, Y. Long, et al., Chem. Commun. 47 (2011) 6695–6697.
[20] Y. Song, K. Qu, C. Zhao, J. Ren, X. Qu, Adv. Mater. 22 (2010) 2206.
[21] M.S. Kim, S. Cho, S.H. Joo, et al., ACS Nano 13 (2019) 4312–4321.
[22] F. Qu, T. Li, M. Yang, Biosens. Bioelectron. 26 (2011) 3927–3931.
[23] Y. Hu, X.J. Gao, Y. Zhu, et al., Chem. Mater. 30 (2018) 6431–6439.
[24] H. Wang, P. Li, D. Yu, et al., Nano Lett. 18 (2018) 3344–3351.
[25] L. Chen, Y. Hernandez, X. Feng, K. Muellen, Angew. Chem. Int. Ed. 51 (2012) 7640–7654.
[26] S. Rostami, A. Mehdinia, A. Jabbari, Mater. Sci. Eng. C: Mater. 114 (2020) 111034.
[27] Z. Pan, N. Liu, L. Fu, Z. Liu, J. Am. Chem. Soc. 133 (2011) 17578–17581.
[28] D.B. Shinde, J. Debgupta, A. Kushwaha, M. Aslam, V.K. Pillai, J. Am. Chem. Soc. 133 (2011) 4168–4171.
[29] Z. Xiang, Q. Dai, J.F. Chen, L. Dai, Adv. Mater. 28 (2016) 6253.
[30] K. Gao, B. Wang, L. Tao, et al., Adv. Mater. 31 (2019) 1805121.
[31] L. Ren, X. Yi, L. Tong, et al., Appl. Catal. B 279 (2020) 119352.
[32] M. Masteri-Farahani, F. Ghorbani, N. Mosleh, Spectrochim. Acta Part A 245 (2020) 118892.
[33] J.H. Yu, C.Z. He, C.Y. Pu, et al., Chin. Chem. Lett. 32 (2021) 3149–3154.
[34] H.Y. Yang, C.Z. He, L. Fu, et al., Chin. Chem. Lett. 32 (2021) 3202–3206.
[35] R. Wang, C.Z. He, W.X. Chen, C.X. Zhao, J.R. Huo, Chin. Chem. Lett. (2021), doi:10.1016/j.cclet.2021.05.024.
[36] H. Yan, L. Wang, Y. Chen, et al., Research (2020) 1–11.
[37] Y. Chen, L. Jiao, H. Yan, et al., Anal. Chem. 92 (2020) 13518–13524.
[38] D.V. Kosynkin, A.L. Higginbotham, A. Sinitskii, et al., Nature 458 (2009) 872–875.
[39] Z. Zhang, Y. Li, S. Zhu, et al., Chin. Chem. Lett. 30 (2019) 505–508.
[40] R. Bi, R. Zhang, J. Shen, et al., J. Membr. Sci. 572 (2019) 504–511.
[41] A. Yazdi, K. Chizari, A. Jalilov, J. Tour, U. Sundararaj, Anal. Chem. 92 (2020) 5319–5328.
[42] D. Zhang, Q. Ma, H. Fan, H. Yang, S. Liu, Carbon 71 (2014) 120–126.
[43] R. Zhang, C.L. Sun, Y.J. Lu, W. Chen, Anal. Chem. 87 (2015) 12262–12269.
[44] Y. Zheng, Y. Jiao, L. Ge, M. Jaroniec, S.Z. Qiao, Angew. Chem. Int. Ed. 52 (2013) 3110–3116.
[45] C.H. Choi, M.W. Chung, H.C. Kwon, S.H. Park, S.I. Woo, J. Mater. Chem. A 1 (2013) 3694–3699.
[46] H. Tabassum, W. Guo, W. Meng, et al., Adv. Energy Mater. 7 (2017) 1601671.
[47] Y. Liu, M. Zhou, W. Cao, et al., Anal. Chem. 91 (2019) 8170–8175.
[48] C. Wang, Y. Shi, Y.Y. Dan, et al., Chem. Eur. J. 23 (2017) 6717–6723.
[49] W. Hu, M.R. Younis, Y. Zhou, C. Wang, X.H. Xia, Small 16 (2020) 2000553.
[50] A. Byeon, J.W. Lee, J. Phys. Chem. C 117 (2013) 24167–24173.
[51] R. Zhang, C. Zhang, F. Zheng, et al., Carbon 126 (2018) 328–337.
[52] Y. Gong, H. Fei, X. Zou, et al., Chem. Mater. 27 (2015) 1181–1186.
[53] D.J. George, S. Halabi, T.F. Shepard, et al., Clin. Cancer Res. 11 (2005) 1815–1820.
[54] R. Yu, W. Ma, X. Liu, et al., Theranostics 6 (2016) 1732–1739.